# Final report of project NKFIH K-115959 "Pattern formation in far-from-equilibrium systems" (Duration: 01.01.2016 to 31.12.2019)

# I. Introduction:

**Aims:** Nanoscale self-assembly often results in complex multi-scale patterns, where the link between the properties of the large-scale structure and the building blocks is not immediately straightforward. These could be used to engineer materials for specific uses provided that self-assembly can be controlled. A detailed understanding of the relevant processes is needed to achieve this. The present proposal is aimed at developing mathematical models based on classical density functional theory of classical particles and the phase field approach working with coarse grained order parameters that extend modeling to the description of different examples of crystalline self-assembly hitherto unaddressed. The selection of the specific problems is motivated by the requirements that (i) they should be complex, (ii) interesting both from scientific and application viewpoints, (iii) visually pleasing, (iv) exemplify the diversity of the pattern formation processes, and (v) their treatment needs a specific extension/adaptation of the existing continuum models, pushing theory beyond the present limits. The problems chosen incorporate, among others, complex nucleation processes, biomorphic/biological crystallization, nanoscale eutectics, pattern formation by photosynthesizing bacteria.

**Working hypothesis:** Starting from the existing atomistic and coarse-grained field theoretic models it is possible to work out predictive mathematical models that are able to describe a variety of pattern formation processes of hitherto unseen complexity.

# II. Results

## 1. Molecular scale modeling of nucleation phenomena:

We studied homogeneous and heterogeneous nucleation phenomena using a simple classical density functional theory (termed Phase-Field Crystal or PFC model) both with dominantly diffusive or hydrodynamic relaxation (DPFC and HPFC) respectively. The latter is based on combining the PFC model with fluctuating nonlinear hydrodynamics. Using these molecular scale techniques, we addressed microscopic aspects of exotic nucleation modes, such as amorphous precursor mediated heterogeneous nucleation, athermal nucleation induced by foreign particles, and growth front nucleation (GFN) during which new crystal grains are created at the perimeter of the growing crystals. The respective results were published in Refs. [1,4,8-10,23]. A brief summary of the main findings is given below:

***(a)*** ***Amorphous precursors:*** Our previous work with DPFC models indicated that nucleation of amorphous precursor clusters assists the formation of the stable crystalline phase. In the framework of the present project, we explored the structural aspects of this phenomenon (Fig. 1) [1,9,23]. Following methods used in analyzing molecular dynamics and colloid experiments, we employed the $Q_6$ bond-order parameter to classify the emerging solid neighborhoods into three categories: amorphous ($Q_6 < 0.28$), medium range crystallike order (MRCO: $0.28 < Q_6 < 0.4$), BCC crystalline ($0.4 < Q_6$). We found that during homogeneous nucleation the amorphous and MRCO domains appear simultaneously, before the BCC structure starts to form on their surfaces (Fig. 2a) [9,23]. The $Q_6$ vs. $Q_4$ bond order parameter map indicates that the amorphous structure of the single mode PFC model is close to the structure of the Lennard-Jones liquid from molecular dynamics simulations (*cf.* Figs.2b and 2c) [9,23]. Finally, the pair correlation function for amorphous Fe the PFC model predicts has a striking similarity to the results from molecular dynamics simulations [23].

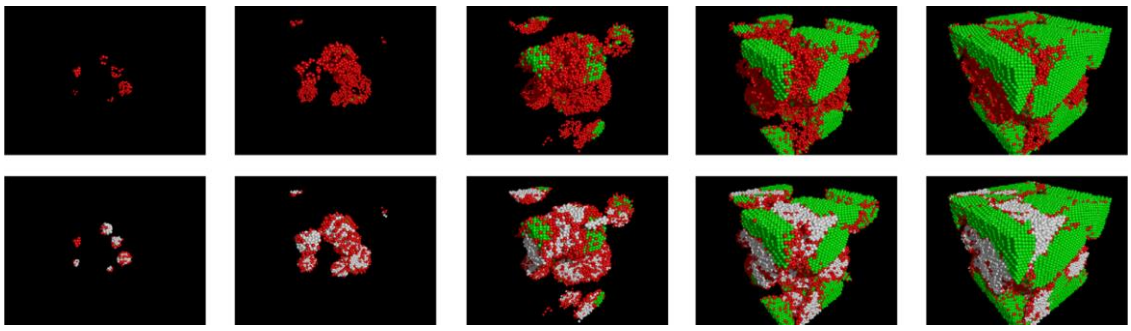

**Fig. 1:** Structural analysis of two-step nucleation observed in a DPFC simulation in terms of the $Q_6$ bond order parameter [9]. (Liquid – transparent; white – amorphous; red – MRCO; green – BCC crystalline.) Time elapses from left to right. Amorphous domains are not show in the upper row.

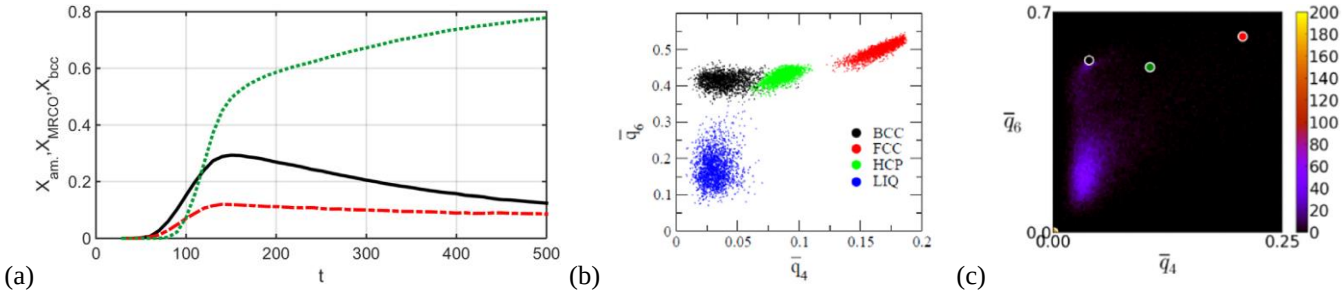


**Fig. 2:** Structural analysis of two-step nucleation observed in a DPFC simulation (a) phase fractions as a function of time for Fig. 1 (black line – amorphous; red line – MRCO; green line – BCC crystalline) [9]. (b) $Q_6$ vs. $Q_4$ map for the Lennard-Jones system. (c) $Q_6$ vs. $Q_4$ map for the amorphous clusters occurring in the DPFC simulations [9].

***(b)*** ***<u>Particle induced athermal nucleation:</u>*** In this process foreign particles initiate crystallization beyond a critical undercooling. According to macroscopic theory, for undercoolings smaller than the critical one, the foreign particle is covered by an adsorbed crystal, whose shape depends on the shape of the substrate: e.g., for a square substrate, the critical shape is the outer circle drawn around the square. In a previous work, we investigated this mechanism in detail by solving the Euler-Lagrange equation of the PFC, and found a different behavior: the critical shape preceding free growth for a square substrate is not the external circle, but a "flowerlike" object with half circles on each side. In the present work performed dynamic simulations, under isothermal and cooling conditions assuming both (colloid-like) diffusion controlled [9,23] and (simple fluid-like) hydrodynamic [4,8-10,23] density relaxation. We found that contrary to the prediction of analytic theory, the "flowerlike" morphology was stable. The deviation from analytic theory originates from the grain boundaries forming at the corners of the substrate due to the fact that differently oriented crystallites on the neighboring faces of the substrate, a feature that stabilizes the corners.

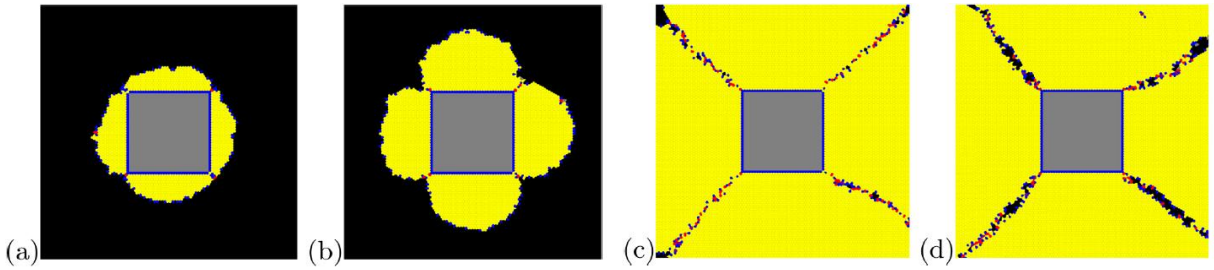


**Fig. 3:** Stable and free growth stages of particle induced crystallization on a square substrate in HPFC simulations. The undercooling increases from left to right. Voronoi polyhedral map is shown: Voronoi cells for atoms with 4, 5, 6, and 7 crystal neighbors are colored gray, red, yellow, and blue. The unperturbed crystal has a triangular structure, whereas the substrate has a square lattice of the same lattice constant [8].

***(c)*** ***<u>Growth front nucleation (GFN):</u>*** is a process, in which new grains form at the propagating solidification front, and identified as the mechanism by which complex polycrystalline growth forms such as spherulites, disordered dendrites, crystal sheaves, etc. GFN has been successfully modeled by phase-field methods relying on an orientation field that describes the local crystallographic orientation. In this approach, the formation of new grains happens either by quenching orientational defects (bundles dislocations) into the crystal, or via branching in the directions of low grain-boundary energies. We addressed the formation of new (differently oriented) crystal grains at the solid-liquid interface in far-from-equilibrium liquids within the framework of the hydrodynamic PFC (HPFC) model [4,8-10,23]. Two mechanisms were identified (Fig. 4): (i) quasi-periodic formation of misfit dislocations in cusps of the solid-liquid interface that emerge via an analogue of the stress induced Asaro-Tiller-Grifeld instability, yielding dislocation chains, and (ii) preferred nucleation ahead of the growth front, induced by the interference of density waves emanating from the solid-liquid interface [4-6]. The latter phenomenon resembles the formation of "satellite" crystals in the vicinity of existing crystals, a process observed in a molecular dynamics simulation in highly undercooled iron liquid containing 1 billion atoms. In large scale simulations, these processes lead to spherulite-like nanostructures.

***(d)*** <u>Crystallization kinetics in HPFC model:</u> At high undercoolings, the crystalline fraction follows the Johnson-Mehl-Avrami-Kolmogorov relation with kinetic exponent $p = 3.31 \pm 0.03$ that indicates a slightly increasing nucleation rate combined with steady state growth in 2D.

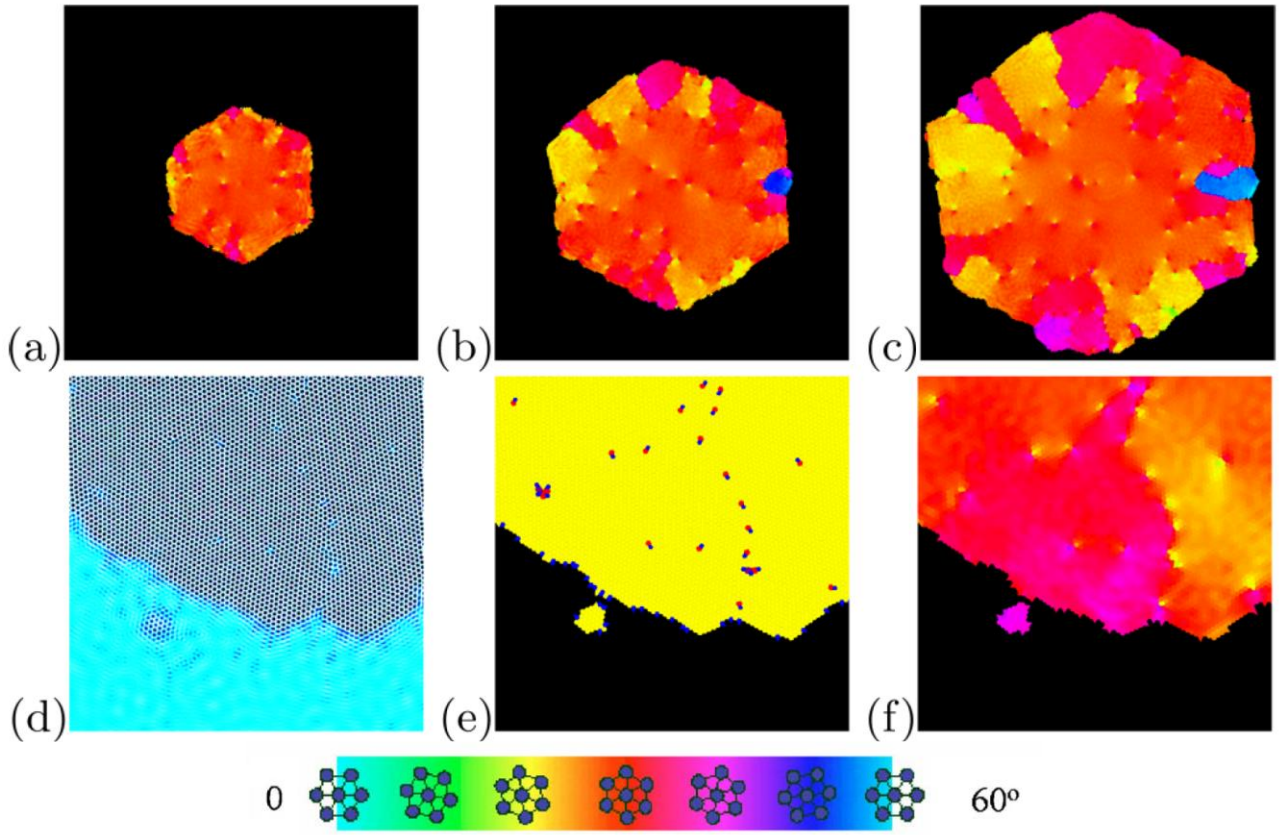


**Fig. 4:** Growth front nucleation (GFN) as predicted by the hydrodynamic PFC model [8]. (a)-(c) Orientation map of the growing crystal. (Different colors stand for different orientations; see bottom row.) (d)-(f) Illustrations of the two GFN mechanisms: (d) particle density, (e) Voronoi map (the blue-red pairs indicate dislocations), (f) orientation map.

## 2. Phase transitions in coarse-grained phase-field and more complex models:

***(a)*** ***<u>Grain coarsening and complex growth forms in orientation field based models:</u>*** We used two orientation field based models (by Kobayashi et al.: KWC, and Henry et al.: HMP) to address polycrystalline solidification and growth in 2D. We found that both models can describe a range of polycrystalline growth morphologies equally well (e.g., dendritic structure disordered by foreign particles, Fig. 5a) and that they lead to similar limiting distribution for the grain size (Fig. 5b), which is in a good agreement with distributions obtained by a range of other methods such as $Q$ = 72 Potts model, multiphase-field methods, surface solver, etc. Remarkably the lognormal limiting distribution obtained from experiments performed on thin metallic films differ considerably.

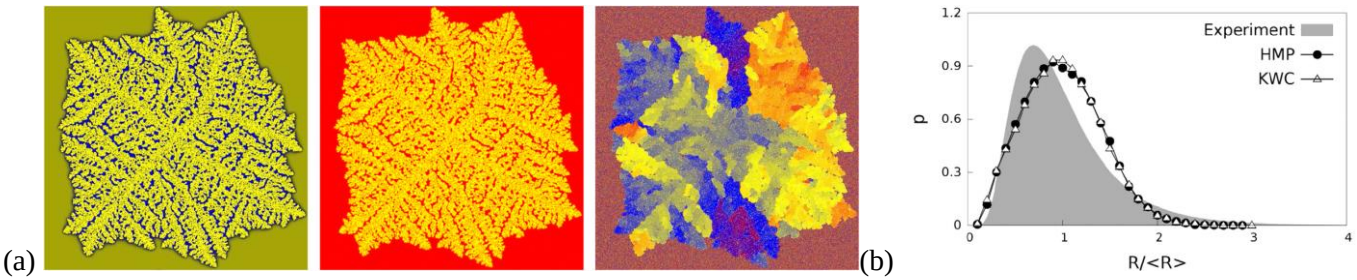


**Fig. 5:** Polycrystalline growth and grain coarsening as predicted by the orientation field model of Henry et al. [6]. (a) Dendritic structure disordered by foreign particles (concentration-, phase-, and orientation fields are shown); (b) Long-time limiting distribution of the grain size for the two orientation field models and the experimental distribution for thin metallic films.

We investigated possible origins of the observed differences in the limiting distributions. We observed that the orientation field models are prone to topological defects due to the extended solid-liquid interface, which defects sometimes lead to the pinning of grain boundaries, influencing thus grain coarsening. We developed two orientation field models that remove this difficulty [5], and demonstrated that adding appropriate noise to the equation of motion of the orientation field can also remove pinning. We then investigated the effect of how the

detection of low angle grain boundaries influences the limiting size distribution. It has been shown that excluding an increasing amount of the lowest angle of the misorientations, there is a continuous transition from the theoretical limiting distribution to the experimentally observed lognormal distribution (Fig. 6) [7]. This suggests that either some of the low angle grain boundaries are not resolved in the experiments, or they are indeed missing.

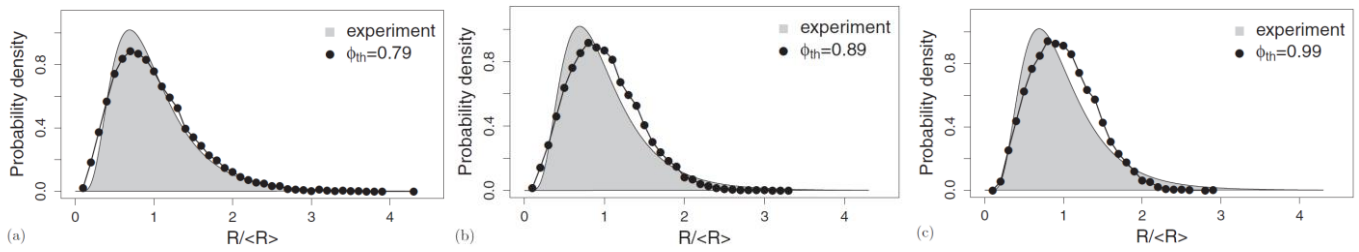


**Fig. 6:** Effect of the lowest angle grain boundaries on the limiting grains size distribution [7]. On the left about 10% of the lowest misorientations are left out of the evaluation.

***(b)*** ***Solidification and melt flow:*** Casting methods are widely used for producing metal components. The cast product solidifying in the mold is usually polycrystalline, i.e., it is composed of a large number of crystallites. Its mechanical and other properties are determined by size-, shape-, and composition distributions of the crystallites, known as the microstructure. The melt flow and the motion of the growing crystallites play an essential role in determining the microstructure that evolves in casting. Combining the phase-field theory of solidification with the lattice Boltzmann technique for simulating melt flow, we developed a computer model that is able to handle growing crystals that move in melt flow [24]. To handle mobile particles, an overlapping multigrid scheme was developed, in which each individual crystal particle has its own grid moving with the particle. The equations describing the growth of the crystal particles are solved on their own grids, and are moved according to the lattice Boltzmann equations solved on a global grid. Using this approach, we modeled model the columnar to equiaxed morphological transition in an Al–Ti alloy important for aerospace and automotive applications (Fig. 7).

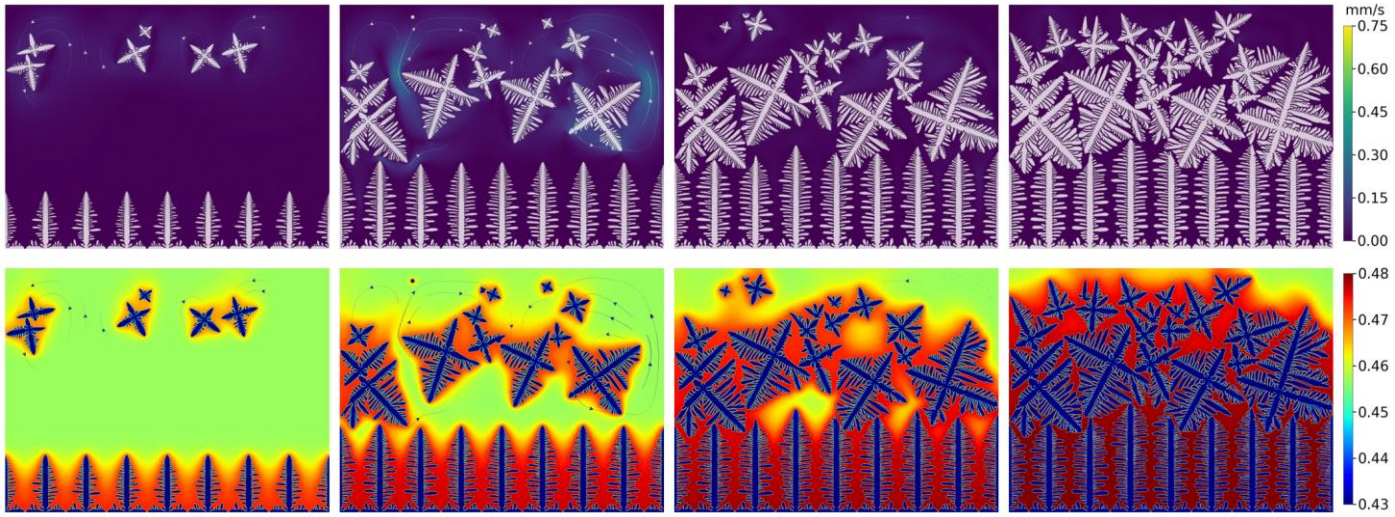


**Fig. 7:** Snapshots of the velocity and concentration fields (upper and bottom rows, respectively) during columnar to equiaxed transition via columnar growth from the bottom and nucleation in the upper domain of the simulation box [24]. The time elapses from left to right. The simulation was performed on a 4096 × 3072 grid.

***(c)*** ***Phase-field modeling of complex 3D patterns in eutect systems:*** We used a relatively simple phase-field model address anisotropic eutectic freezing on the nanoscale in two and three dimensions [12]. Comparing parameter-free simulations with experiments, we demonstrated that the model is quantitative for Ag–Cu. We explored the effect of material properties and the conditions of freezing on eutectic pattern formation. It was found that the anisotropies of kinetic coefficient and the (solid–liquid and solid–solid) interfacial free energies, the crystal misorientation relative to pulling, and the lateral temperature gradient play essential roles in determining the eutectic pattern. We also reproduced eutectic morphologies that form when one of the solid phases are faceted, and investigated cases, in which the kinetic anisotropy for the two solid phases is drastically different [25].

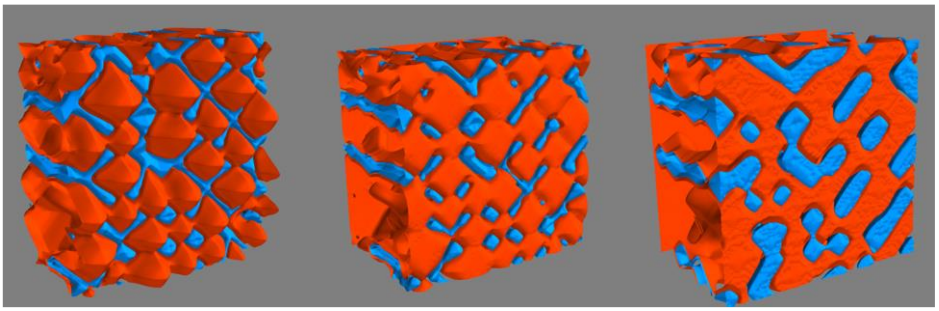

**Fig. 8:** Quantitative 3D phase-field simulations showing the effect of the temperature gradient on the nanoscale eutectic pattern in a highly undercooled system, where one of the phases (the blue one) has a large anisotropy of the solid-liquid interfacial free energy [25]. The temperature gradient increases from left to the right, flattening the solid-liquid interface.

***(d)*** ***Pattern formation in biological systems:*** We addressed different biological systems, including self-organization of light emitting bacteria and microstructure evolution in mollusk shells.

*(i)* Antenna systems absorb light and transmit excitation energy to the reaction center (RC) in *photosynthetic organisms*. As the emitted (bacterio)chlorophyll fluorescence competes with the photochemical utilization of the excitation, the measured fluorescence yield is informed by the migration of the excitation in the antenna. In this work, the fluorescence yield concomitant with the oxidized dimer (P+) of the RC were measured during light excitation (induction) and relaxation (in the dark) for whole cells of photosynthetic bacterium Rhodobacter sphaeroides lacking cytochrome c2 as natural electron donor to P+ (mutant cycA). The relationship between the fluorescence yield and P+ (fraction of closed RC) showed deviations from the standard Joliot-Lavergne-Trissl model: 1) the hyperbola is not symmetric and 2) exhibits hysteresis. These phenomena originate from the difference between the delays of fluorescence relative to P+ kinetics during induction and relaxation, and in structural terms from the non-random distribution of the closed RCs during induction. The experimental findings are supported by Monte Carlo simulations (Fig. 9) and by results from statistical physics based on random walk approximations of the excitation in the antenna. The applied mathematical treatment demonstrates the generalization of the standard theory and sets the stage for a more adequate description of the long-debated kinetics of fluorescence and of the delicate control and balance between efficient light harvest and photoprotection in photosynthetic organisms. (Manuscript submitted to Scientific Reports.)

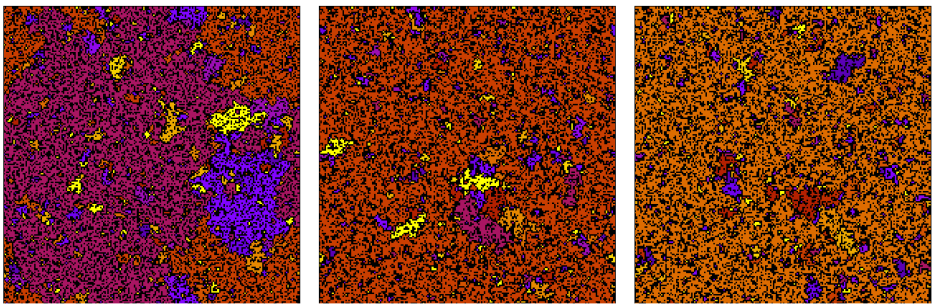

**Fig. 9** Typical cluster structures of reaction centers from Monte Carlo simulations on a 200 × 200 square lattice at an occupation probability, slightly above the site-percolation threshold. Left panel: uncorrelated percolation, corresponding to the structure during relaxation with $n = 1$. Middle panel: during induction with hopping probability $p = 0{:}9$ and step number $n = 2$. Right panel: during induction with $p = 0{:}9$ and $n = 3$. Sites with the same colour represent connected clusters of closed RCs.

*(ii)* *Mollusk shells* are regarded as a classic model system for studying the formation–structure–function relationships during biomineralization, a process that yields hierarchically structured organic-inorganic composite structures in living organisms. Typically, the mollusc shells consist of a number of highly mineralized ultrastructures of complex mineral–organic architecture. Remarkably, shells of mollusc species from different classes display similar ultrastructural motifs. These hierarchically organized biocomposites in many cases provide enhanced strength and toughness compared to the pure mineral phase and superiority compared to modern man-made composites. We explored the possibility of applying phase-field modeling for the description of the globular, prismatic, and nacreous ultrastructures observed in mollusk shells. This work was done in collaboration with I. Zlotnikov and his team at the Institute of Molecular Bioengineering, Technical university Dresden, who provided the experimental data and the biological background. A minimum model was proposed that qualitatively describes all three types of the microstructure (Fig. 10) [21,25]. Based on this observation,

architectural constraint is proposed for the evolution of molluscan shells: the morphospace of possible shell ultrastructures is bounded by the thermodynamic and kinetic limitations of directional solidification [25].

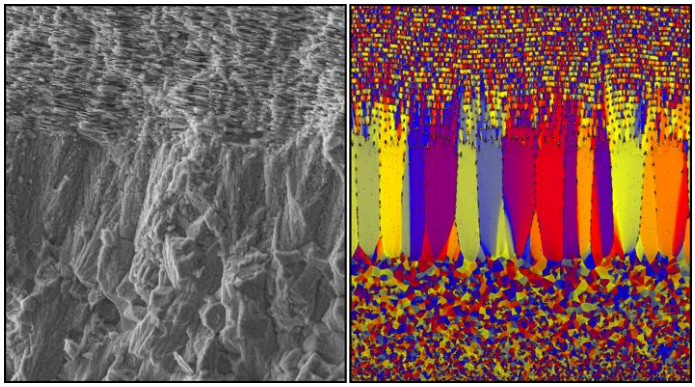

**Fig. 10:** Cross-sectional change of the shell microstructure (left) in the electron microscope image of the shell of *Nautilus pompilius*, and (right) the simulated microstructure predicted by the phase-field theory (different colors indicate different crystallographic orientations). Growth direction is upwards. Note the following sequence of morphological transitions in both panels: granular → columnar → nacre [25].

***(e)*** ***Pattern formation in phase separating systems:*** Solidification is often preceded by phase separation whose spatial distribution influences later stage pattern formation. Within the framework of the present project, we addressed to relevant cases: (i) we combined a physically consistent multiphase-field theory, which we developed recently, with incompressible hydrodynamics and applied it for complex phase separation problems [2], and (ii) investigated phase separation in a binary case where the two phases have a viscosity contrast [19,22]. The latter work was done in collaboration with H. Henry, École Polytechnique, Palaiseau, France.

*(i) Multiphase-field model:* Our model creates equilibrium planar binary interfaces without the appearance of a third phase, while the contact angle measurements resulted in less than 1.5% relative error compared to the theoretical values. We studied pattern formation in multicomponent system, such as the case of a four-component incompressible Cahn-Hilliard fluid. As shown in Fig. 11, asymmetric interfacial data, diffusion constants and viscosities lead to the formation of patterns known in microfluidics, while the third phases appeared dynamically indeed tend to vanish yielding eventually binary interfaces. Deeper understanding of the underlying microscopic phenomena may offer new routes for designing novel materials, and generate knowledge that might play a crucial role in various fields ranging from advanced drug delivery to combined crude oil recovery / $CO_2$ storage.

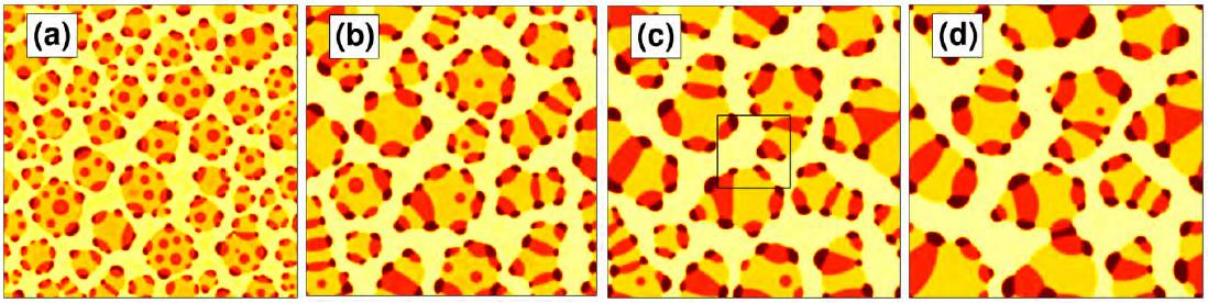


**Fig. 11:** Time evolution of phase separation in an asymmetric four-component incompressible Cahn-Hilliard fluid [2].

*(ii) Phase separation vs. viscosity contrast:* We investigated hydrodynamic coarsening in three dimensions of a critical mixture using the Cahn-Hilliard/Navier-Stokes model (Fig. 12). The topology of the resulting intricate bicon-tinuous microstructure is analyzed through the principal curvatures to prove self-similar morphological evolution. We found that both the isoviscous and the variable viscosity systems evolve in self-similar way, however, the two systems have a distinct topological character [19]. It appears, however, that the self-similar bicontinuous morphology is robust only for moderate departure from the perfectly symmetric case. In contrast, the connectivity of one phase decreases when its volume fraction decreases or when it becomes less viscous than the complementary phase. Eventually the self-similarity breaks down [22].

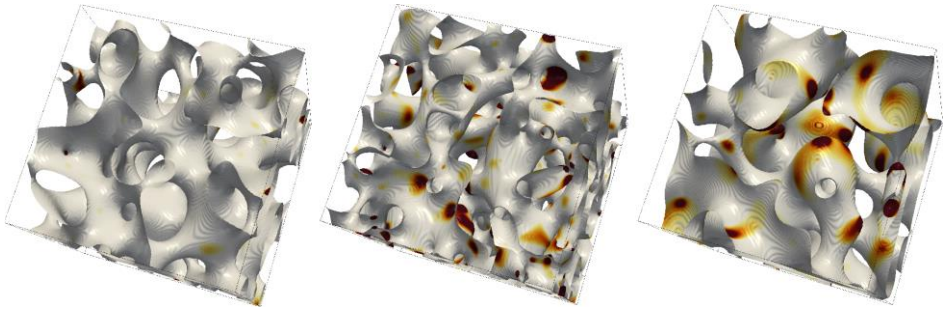

**Fig. 12:** Typical images of the interface between the phases for different values of the parameters [22]. The color of the surface indicates the Gaussian curvature (clear or yellow: negative or zero; red or dark: positive). The volume fraction of the minority phase is 0.6 and the viscosity of the minority phase is equal to the viscosity of the majority (left), 16 times smaller (center) and 128 times smaller (right). Regions with positive Gaussian curvature are more frequent in the latter case.

### *(f)* ***Phase transitions in disordered systems:***

*(i)* We studied phase transitions of the ferromagnetic *q-state Potts chain with random nearest-neighbor couplings* having a variance $\Delta^2$ and with homogeneous long-range interactions, which decay with the distance as $r$ to the power of $-(1+\sigma)$, $\sigma > 0$. We observed by numerical calculation that the phase transition stays first order for $\sigma < \sigma c(\Delta) \leq 0.5$, while the correlation length becomes divergent at the transition point for $\sigma c(\Delta) < \sigma < 1$. In the latter regime the average magnetization is continuous for small enough $\Delta$, but, for larger $\Delta$, it is discontinuous at the transition point, thus the phase-transition is of mixed order [3].

*(ii)* We studied the time evolution of the average magnetization of the *random quantum Ising chain after sudden change of the parameters (quantum quench)*. We observed different relaxation behavior for quenches starting from different initial states to the critical point. Starting from a fully ordered initial state, the relaxation is logarithmically slow in time. Starting from a fully disordered initial state, the magnetization stays at zero for a period of time and then starts to increase until it saturates to an asymptotic value. The distribution of long-time limiting values of the magnetization shows that the typical and the average values scale differently and the average is governed by rare events. [11]

*(iii)* We studied the *entanglement of composite systems* that consist of a clean subsystem and a random subsystem, both being critical. In the composite, antiferromagnetic XX-chain with a sharp interface, the entropy is found to grow in a double-logarithmic fashion $S \sim \ln \ln(L)$, where $L$ is the length of the chain. These results are explained through strong-disorder RG arguments. [14]

*(iv)* The *strong disorder renormalization group (SDRG) method* is a very efficient procedure to study the critical properties of different (quantum, classical, stochastic) systems in the presence of quenched disorder. We wrote a review article in which we describe the recent developments of the method. [17]

*(v)* We calculated the *connected transverse-spin correlation function of the random quantum Ising model* by a numerical implementation of the SDRG method in $d = 1$, 2 and 3 dimensions. At the critical point an algebraic decay with an exponent $\eta$ is found, which is approximately $\eta \approx 2 + 2d$. [18]

*(vi)* We studied the *entanglement entropy of random partitions in one- and two-dimensional critical fermionic systems*. In an infinite system, we considered a finite, connected (hypercubic) domain of linear extent L, the points of which with probability $p$ belong to the subsystem. The leading contribution to the average entanglement entropy is found to scale proportionally to the volume, with an additive logarithmic correction term. In one dimension, the prefactor of the correction is determined by the central charge of the model and a universal function of $p$. In two dimensions, the prefactor has a different functional form of $p$ below and above the percolation threshold. [26]

*(vii)* We studied the *quantum Ising chain with uniformly distributed random antiferromagnetic couplings* ($1 < J_i < 2$) and uniformly distributed random transverse fields ($\Gamma_0 < \Gamma_i < 2\,\Gamma_0$) in the presence of a homogeneous longitudinal field, $h$. Using different numerical techniques (DMRG, combinatorial optimisation and strong disorder RG methods) we explore the phase diagram, which consists of an ordered and a disordered phase. At one end of the transition line ($h = 0$, $\Gamma_0 = 1$) there is an infinite disorder quantum fixed point, while at the other end ($h = 2$, $\Gamma_0 = 0$) there is a classical random first-order transition point. Close to this fixed point, for $h > 2$ and $\Gamma_0 > 0$ there is a reentrant ordered phase, which is the result of quantum fluctuations by means of an order through disorder phenomenon. [27]

***(g) Phase transitions in other complex systems (multiple junctions, supersolid state, surface criticality):***

*(i)* The *contact process* is one of the basic problems of non-equilibrium phase transitions. Here we considered this problem *in a multiple junction geometry*, which is composed of $M$ semi-infinite chains having a common starting site. As opposed to the continuous transitions of the translationally invariant ($M = 2$) and the semi-infinite ($M = 1$) system, the local order parameter is found to be discontinuous for $M > 2$. The temporal correlation length diverges algebraically at the critical point thus the transition is of mixed order. [13]

*(ii) Dynamically generated supersolid states:* We have introduced a model of hard-core bosons in the presence of short- and long-range interactions, which has experimental relevance in cold atomic systems. The one-dimensional problem is solved exactly in the thermodynamic limit and Mott insulator (MI), density wave (DW) and superfluid (SF) phases are identified. We have also determined the quantum relaxation properties of the system after sudden quenches and - among others - we have identified a dynamically generated supersolid state. [15]

*(iii)* We have considered the *quantum XX model in the presence of competing nearest-neighbor and global-range interactions*, which is equivalent to a Bose-Hubbard model with cavity mediated global-range interactions in the hard-core boson limit. Using fermionic techniques, the problem is solved exactly in one dimension in the thermodynamic limit. The ground state phase diagram consists of two ordered phases: ferromagnetic (F) and antiferromagnetic (AF), as well as an XY phase having quasi-long-range order. We have also studied quantum relaxation after sudden quenches. Quenching from the AF phase to the XY region remanent AF order is observed below a dynamical transition line. In the opposite quench, from the XY region to the AF phase beyond a static metastability line AF order arises on top of remanent XY quasi-long-range order, which corresponds to dynamically generated supersolid state in the equivalent Bose-Hubbard model with hard-core bosons. [16]

*(iv)* We studied the *surface critical behavior of the contact process near an extended surface defect*, where the local control parameter deviates from the bulk one by an amount which is decays as a power s of the distance from the surface. We concentrate on the marginal situation $s = 1/\nu_\perp$, where $\nu_\perp$ is the critical exponent of the spatial correlation length. The system exhibits a rich surface critical behavior. For weaker local activation rates the phase transition is continuous, having an order-parameter critical exponent, which varies continuously with the prefactor $A$. For stronger local activation rates the phase transition is of mixed order: the surface order parameter is discontinuous; at the same time the temporal correlation length diverges algebraically as the critical point is approached. [20]

# III. Scientometry

During the four years of the project (2016-2019), 26 scientific publications appeared, of these 23 in refereed journals, 2 extended abstracts, 1 book chapter. Furthermore, 1 manuscript is accepted for publication in a refereed journal, while 1 manuscript is under evaluation in another refereed journal. The **sum of impact factors** for the appeared and accepted papers is **118.689**. We are aware of about 70 independent citations so far to these works. During the project we had 22 invited talks at international conferences and workshops (of which 2 were plenary talk), and we are to deliver yet 4 more invited talks scheduled for 2020 that are related to the results of the present project. Three PhD dissertations were made of the matter of the project.

## Publications:


[1] F. Podmaniczky, G.I. Tóth, T. Pusztai, L. Gránásy: Investigating nucleation using the phase-field method, J. Ind. Inst. Sci. 96, (3) 161-177, 2016
IF: 0.857

[2] G.I. Tóth, T. Pusztai, B. Kvamme, L. Gránásy: A physically consistent multiphase-field theory of first order phase transitions, Collection of Extended Abstracts, Frontiers in Solidification, TMS Annual Meeting, eds. W. Kurz, J. Dantzig, A. Karma, J. Hoyt (EPFL, Lausanne, Switzerland), pp. 73-76, 2016
IF: -

[3] J-Ch. Anglès d'Auriac, F. Iglói: Phase-transitions of the random bond Potts chain with long-range interactions, Phys. Rev. E 94, 062126, 2016
IF: 2.252

[4] L. Gránásy, F. Podmaniczky, G.I. Tóth: Phase-field crystal modeling of nucleation including homogeneous and heterogeneous processes and growth front nucleation, Collection of Extended Abstracts, Frontiers in Solidification, TMS Annual Meeting, eds. W. Kurz, J. Dantzig, A. Karma, J. Hoyt (EPFL, Lausanne, Switzerland), pp. 23-26, 2016
IF: -

[5] B. Korbuly, M. Plapp, H. Hervé, J.A. Warren, L. Gránásy, T. Pusztai: Topological defects in two-dimensional orientation-field models for grain growth, Phys. Rev. E 96, 052802 (pp. 1-16), 2017
IF: 2.366

[6] B. Korbuly, T. Pusztai, G.I. Tóth, H. Hervé, M. Plapp, L. Gránásy: Orientation- field models for polycrystalline solidification: grain coarsening and complex growth forms, J. Cryst. Growth 457, 32-37, 2017
IF: 1.751

[7] B. Korbuly, T. Pusztai, H. Hervé, M. Plapp, M. Apel, L. Gránásy: Grain coarsening in two-dimensional phase-field models with an orientation field, Phys. Rev. E. 95, (5) 053303 (pp. 1-12), 2017
IF: 2.366

[8] F. Podmaniczky, G.I. Tóth, G. Tegze, T. Pusztai, L. Gránásy: Phase-field crystal modeling of heteroepitaxy and exotic modes of crystal nucleation., J. Cryst. Growth 457, 32-37, 2017
IF: 1.751

[9] F. Podmaniczky, G.I. Tóth, G. Tegze, L. Gránásy: Hydrodynamic theory of freezing: Nucleation and polycrystalline growth, Phys. Rev. E. 95, (5) 052801 (pp.1-8), 2017
IF: 2.366

[10] F. Podmaniczky, G.I. Tóth, L. Gránásy: Nucleation and polycrystalline growth in a hydrodynamic theory of freezing, Proc. 6th Decennial Int. Conf. on Solidification Processing, ed. Z. Fan, Brunel University, London, pp. 22-25, ISBN – 978-1-908549-29-7, 2017
IF: -

[11] G. Roósz, Y.-C. Lin, F. Iglói: Critical quench dynamics of random quantum spin chains: Ultra-slow relaxation from initial order and delayed order from initial disorder, New J. Phys. 19, art. no. 023055 (pp. 1-11), 2017
IF: 3.786

[12] L. Rátkai, G.I. Tóth, L. Környei, T. Pusztai, L. Gránásy: Phase-field modeling of eutectic structures on the nanoscale: the effect of anisotropy., J. Mater. Sci. 52, (10) 5544-5558, 2017
IF: 2.599

[13] R. Juhász, F. Iglói: Mixed-order phase transition of the contact process near multiple junctions, Phys. Rev. E 95, art. no. 022109 (pp. 1-8), 2017
IF: 2.366

[14] R. Juhász, I. A. Kovács, G. Roósz, F. Iglói: Entanglement between random and clean quantum spin chains, J. Phys. A: Math. Theor. 50, art. no. 324003 (pp. 1-20), 2017
IF: 1.857

[15] B. Blass, H. Rieger, G. Roósz, F. Iglói: Quantum relaxation and metastability of lattice bosons with cavity-induced long range interactions, Phys. Rev. Lett. 121, art. no. 095301 (pp. 1-6), 2018
IF: 8.839

[16] F. Iglói, B. Blass, G. Roósz, H. Rieger: Quantum XX-model with competing short- and long-range interactions: Phases and phase transitions in and out of equilibrium, Phys. Rev. B 98, art. no. 184415 (pp. 1-15), 2018
IF: 3.813

[17] F. Iglói, C. Monthus: Strong disorder RG approach - a short review of recent developments, Eur. Phys. J. B 91, art. no. 290 (pp. 1-25), 2018
IF: 1.536

[18] F. Iglói, I. A. Kovács: Transverse spin correlations of the random transverse-field Ising model, Phys. Rev. B 97, art. no. 094205 (pp. 1-6), 2018
IF: 3.813

[19] H. Henry, G. Tegze: Self- similarity and coarsening rate of a convecting bicontinuous phase separating mixture: Effect of the viscosity contrast, Phys. Rev. Fluids 3, art. no. 074306 (pp. 1-9), 2018
IF: 2.021

[20] R. Juhász, F. Iglói: Non-universal and anomalous critical behavior of the contact process near an extended defect, Phys. Rev. E 97, art. no. 012111 (pp. 1-8), 2018
IF: 2.366

[21] V. Schoeppler, L. Gránásy, E. Reich, N. Poulsen, R. de Kloe, P. Cook, A. Rack, T. Pusztai, I. Zlotnikov: Biomineralization as a Paradigm of Directional Solidification: A Physical Model for Molluscan Shell Ultrastructural Morphogenesis, Adv. Mater. 45, art. no. 1803855 (pp. 1-8), 2018
IF: 21.950

[22] H. Henry, G. Tegze: Kinetics of coarsening have dramatic effects on the microstructure: Self-similarity breakdown induced by viscosity contrast, Phys. Rev. E 100, art. no. 013116, (pp. 1-10), 2019
IF: 2.353

[23] L. Gránásy, G.I. Tóth, J.A. Warren, F. Podmaniczky, G. Tegze, L. Rátkai, T. Pusztai: Phase-field modeling of crystal nucleation in undercooled liquids – A review, Prog. Mater. Sci. 106, art. no. 100569, (pp. 1-51), 2019
IF: 23.725

[24] L. Rátkai, T. Pusztai, L. Gránásy: Phase-field lattice Boltzmann model for dendrites growing and moving in melt flow, Nature partner journal - Comput. Mater. 5, art. no. 113, (pp. 1-10), 2019
IF: 9.200

[25] V. Schoeppler, R. Lemanis, E. Reich, T. Pusztai, L. Gránásy. I. Zlotnikov: Crystal growth kinetics as an architectural constraint on the evolution of molluscan shells, Proc. Nat. Acad. of Sci. (U.S.A.) 114, (41) art. no. 2019-07229RR, (pp. 1-10), 2019
IF: 9.58

[26] G. Roósz, I. A. Kovács, F. Iglói: Entanglement entropy of random partitioning, Eur. Phys. J. B 93, art. no. 8 (pp. 1-8), 2020
IF: 1.440

[27] P. Lajkó, J.-Ch. Anglés d'Auriac, H. Rieger, F. Iglói: Reentrant Random Quantum Ising Antiferromagnet, Phys. Rev. B, accepted for publication; https://arxiv.org/abs/1912.06035, 2020
IF: 3.736